Vacuum ultraviolet spectroscopy of Ce^{3+}-doped $SrMgF_4$ with superlattice structure

2006 J. Phys.: Condens. Matter 18 6033

(http://iopscience.iop.org/0953-8984/18/26/021)

INSTITUTE OF PHYSICS PUBLISHING JOURNAL OF PHYSICS: CONDENSED MATTER

J. Phys.: Condens. Matter **18** (2006) 6033–6044 doi:10.1088/0953-8984/18/26/021

Vacuum ultraviolet spectroscopy of Ce^{3+}-doped $SrMgF_4$ with superlattice structure

M Yamaga[1], E Hayashi[1], N Kodama[2], K Itoh[1], S Yabashi[1], Y Masui[1], S Ono[3], N Sarukura[3], T P J Han[4] and H G Gallagher[4]

[1] Department of Electrical and Electronic Engineering, Faculty of Engineering, Gifu University, Gifu 501-1193, Japan
[2] Department of Materials Science and Engineering, Faculty of Engineering and Resource Science, Akita University, Akita 010-8502, Japan
[3] Institute for Molecular Science, Okazaki 444-8585, Japan
[4] Department of Physics, University of Strathclyde, Glasgow G1 1XN, UK

Received 5 January 2006, in final form 9 May 2006
Published 19 June 2006
Online at stacks.iop.org/JPhysCM/18/6033

Abstract

X-ray diffraction of Ce^{3+}-doped $SrMgF_4$ (SMF:Ce) crystals shows a superlattice structure, reflecting the distribution of Ce^{3+} polyhedra centres observed in optical experiments. Optical absorption bands and fluorescence bands from the Ce^{3+} polyhedra centres overlap in the vacuum ultraviolet (VUV) and ultraviolet (UV) regions, respectively, so that wide pumping and tuning ranges are expected for laser operation. The SMF:Ce crystals, as well as the isomorphous $BaMgF_4$, are candidates for a tunable laser gain material with nonlinear properties.

The optical absorption, excitation, and fluorescence bands observed in the SMF:Ce crystals at low temperatures are ascribed to five distinct fluorescent centres. Three centres have well-known Ce^{3+} optical characters, for example, fluorescence with double peaks separated by 2000 cm^{-1} and five resolved absorption/excitation bands. These centres are assigned to Ce^{3+}-polyhedra classified by weak and strong crystal fields as a consequence of the superlattice structure. The other two fluorescence bands observed in the visible region have 1.5–2 times larger linewidths than those of the former three bands. These bands are interpreted as optical transitions from complexes consisting of Ce^{3+} and one or two electrons trapped at a vacancy of the nearest neighbour F^- ligand ions.

1. Introduction

There is much interest in Ce^{3+}-doped ionic crystals for applications in scintillators and ultraviolet (UV) tunable lasers [1, 2]. Operations of optically pumped tunable solid-state lasers in the UV region using the 5d–4f transition of Ce^{3+} in fluoride crystals $LiYF_4$ (LYF) [3] and

$LiCaAlF_6$ (LiCAF) [4] have been reported. Recently, a solid-state laser operating in the vacuum ultraviolet (VUV) region has become necessary for photolithography [5]. $BaMgF_4$ (BMF) crystals doped with Ce^{3+} are a candidate for a UV tunable laser gain material with nonlinear properties [6].

In a previous paper [7], we reported a superlattice structure, and optical and electron-spin resonance (ESR) spectra in BMF crystals codoped with Ce^{3+} and Na^+ ions as charge compensator. The fluorescence and excitation spectra observed in the UV region are interpreted as optical transitions from perfect Ce^{3+} and perturbed Ce^{3+} centres. The former requires the substitution of regular Ba^{2+} ions by a single Ce^{3+} ion; as a consequence, they have different crystal fields originated by the superlattice structure of the BMF crystal. The latter corresponds to Ce^{3+} ions substituting for Ba^{2+} ions, associated with a nearest Na^+ ion [7]. Under intensive UV pumping with the fourth harmonic (266 nm) of a pulsed Nd:YAG laser, the BMF:Ce:Na crystal changed its colour from transparent to brown, resulting in no lasing [8]. The colouration may be due to electron and hole trapping centres created by the intensive UV irradiation [9].

Recently, it was reported that $SrMgF_4$ (SMF) crystals doped with Ce^{3+}, which is isomorphous to BMF, also shows a superlattice structure [10]. There are six different polyhedra consisting of a central Sr^{2+} ion and F^- ligand ions in a unit cell of the SMF crystal. Various Ce^{3+} centres produce inhomogeneous broadening of absorption and fluorescence spectra of Ce^{3+} so that wide pumping and tuning ranges are expected for laser operation. This paper reports the relation between the superlattice structure and the VUV/UV spectroscopic properties of Ce^{3+} ions in the SMF crystal.

2. Crystal structure and experimental procedure

Ce^{3+}-doped SMF crystals were grown in an argon atmosphere by the Bridgman–Stockbarger method. The starting charges were formed from a stoichiometric mixture of SrF_2 (50 mol%) and MgF_2 (50 mol%). Ce^{3+} ions of 0.5 at.% relative to Sr^{2+} ions were added in the charge as dopant.

Crystal structure was determined by x-ray diffraction measured at 300 K using the oscillation mode in the range of $\pm 60°$ for Mo Kα_1 radiation (0.709 26 Å) with a Rigaku T-AXIS RAPID Imaging Plate diffractometer.

The SMF crystals, with monoclinic structure, are represented by the point group $P112_1$ [10, 11]. The lattice constants were determined to be $a = 16.925$ Å, $b = 7.4930$ Å, $c = 7.8249$ Å, and $\alpha = 105.71°$ [10]. Ce^{3+} ions prefer to substitute for Sr^{2+} ions in polyhedra composed of F^- ligand ions with approximate C_{2v} symmetry, because the ionic radius (1.11 Å) of Ce^{3+} is close to that (1.13 Å) of Sr^{2+} and larger than that (0.86 Å) of Mg^{2+} [12].

Optical absorption, excitation, and fluorescence spectra were measured in the spectral range 100–600 nm at temperatures in the range 17–300 K using the ultraviolet synchrotron orbital radiation (UVSOR) facility in the Institute for Molecular Science. The absorption and excitation spectra were analysed with a 1 m focal length Seya–Namioka monochromator. The spectral resolution was 0.5–1 nm. Lifetime was measured at room temperature using either a Horiba NAES-700F time-resolved photoluminescence spectrometer at the Instrumental Analysis Centre, Gifu University, or a system consisting of a 1 kHz Ti–sapphire regenerative amplifier with 290 nm, 80 mJ and 210 fs pulses, and a streak camera loaded with a spectrograph. Temperature dependence of the lifetime was measured using a 10 Hz Q-switched Nd:YAG laser operated with 266 nm, 100 mJ and 10 ns pulses and a Hamamatsu Photonics R943-02 photomultiplier connected to a Yokogawa DL1740 digital oscilloscope. Sample temperatures were controlled in the range 13–300 K using a closed-cycle cryorefrigerator.

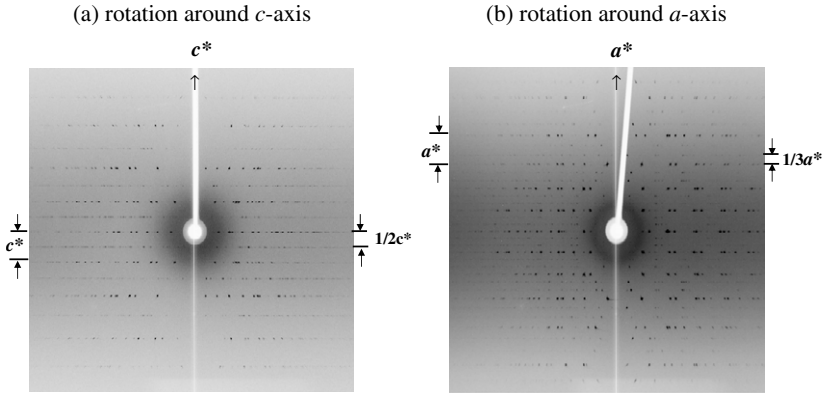

Figure 1. X-ray oscillation photographs taken at 300 K with rotation of the $SrMgF_4$:Ce crystal around (a) the c axis and (b) the a axis.

3. Experimental results

3.1. X-ray diffraction

Figure 1 shows the x-ray oscillation photographs taken with the rotation of the SMF:Ce crystal around the crystalline c and a axes at 300 K. The diffraction spots on horizontal lines correspond to reciprocal lattice vectors in the a^*b^* and b^*c^* planes, and show a typical superlattice structure pattern, which consists of strong main reflections and additional weak satellite reflections. The main reflections are caused by the basic structure with the point group $Cmcm$ [10], whereas the weak satellite reflections are associated with the modulation structure. The satellite spots in figure 1(a) lie midway between two main-reflection layer lines, so the satellites show the reciprocal lattice vector $\frac{1}{2}\boldsymbol{c}^*$. The same superlattice structure pattern for the b^*c^* plane is shown in figure 1(b). These results suggest a commensurate superlattice structure with two-fold and three-fold periodicity along the c and a axes.

Figure 2 shows a unit cell of the SMF crystal with the superlattice structure projected along the c and a axes, suggested by the x-ray diffraction result [10]. The crystal structure is regarded as perovskite-type slabs, which are composed of corner-sharing MgF_6 octahedra and Sr atoms. There are six distinct Sr sites in a unit cell, denoted by Sri (i = 1–6). Lines around Sr denote directions to the nearest neighbour F^- ligand ions. The c-axis projection shows that Sr^{2+} ions are located at the centres of trigonal prisms, whereas the a-axis projection shows that there are several nearest neighbour F^- ligand ions in the c plane including the Sr^{2+} ion.

Figure 3 shows the c-axis projection of the six Sri (i = 1–6) polyhedra in a unit cell of SMF. Solid black circles represent Sr^{2+} ions, grey circles represent F^- ions located at six corners of a trigonal prism, and dark grey circles represent F^- ions in the c plane including the Sr^{2+} ion. Distances between Sr^{2+} and F^- ions are limited to be less than 3.25 Å and are in the range 2.37–3.23 Å. The numbers of F^- ligand ions in Sri (i = 1–6) are 10, 10, 9, 9, 9, and 10, respectively. Tbe crystal field strength for the Sri polyhedra (i = 1–6) increases with decreasing distances between Sr^{2+} and the nearest neighbour ligand ions, increasing number of surrounding ligand ions, and lowering symmetry of the polyhedron. Taking into account the number and the configuration of F^- ligand ions in figure 3, these six Sr polyhedra are approximately classified into two groups of (Sr1, Sr2, Sr6) and (Sr3, Sr4, Sr5), corresponding to strong and weak crystal fields, respectively. The Sr2 polyhedron seems to be slightly different from the Sr1 and Sr6 polyhedra.

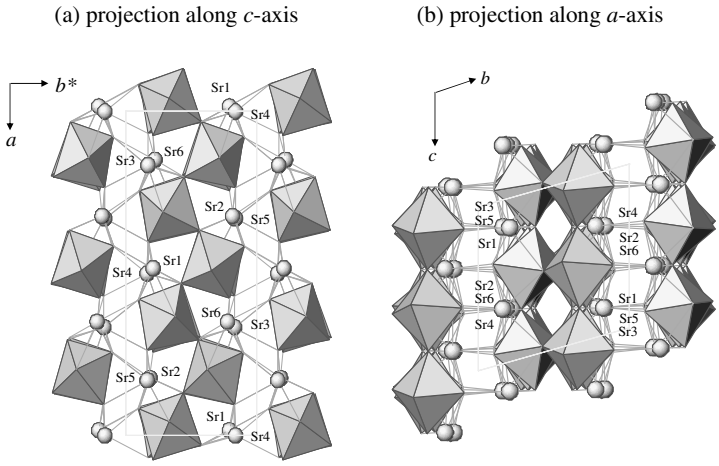

Figure 2. Projection of a unit cell of the $SrMgF_4$ crystal structure along (a) the *c* axis and (b) the *a* axis. Octahedra consist of a central Mg^{2+} ion and six nearest neighbour F^- ligand ions. There are six distinct Sr*i* ($i = 1$–6) sites in a unit cell.

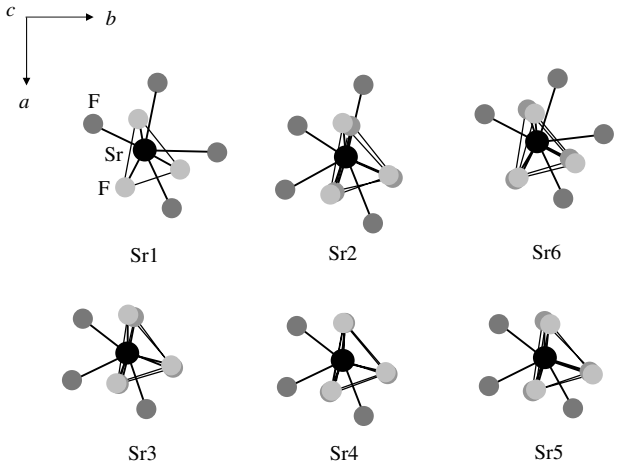

Figure 3. Projection of six different polyhedra Sr*i* ($i = 1$–6) along the *c* axis; they consist of a central Sr ion and F ligand ions. Sr^{2+} ions located at the centre of trigonal prisms are denoted by solid black circles. Grey circles represent F^- ions located at six corners of a trigonal prism, and dark grey circles represent F^- ions in the C plane including the Sr^{2+} ion. Lines around Sr denote directions to the nearest neighbour F^- ligand ions.

3.2. Optical spectra

The optical absorption spectrum of the SMF:Ce crystal measured at 17 K using the UVSOR facility, as shown at the top of figure 4, consists of four intense broadbands at 142, 157, 185 and 200 nm in the VUV region, and several weak bands at 215, 243, 250, 275, 280, 300, and 310 nm in the UV region. Five different fluorescence bands with double peaks, denoted by A, B, C, D and E, are obtained when the crystal is excited at 243, 250, 280, 140 and 185 nm, respectively. These fluorescence bands shift to longer wavelengths in alphabetical order.

The excitation spectrum for the high energy component ($\lambda_{em} = 280$ nm) of the A fluorescence band in figure 4 is clearly resolved into five peaks at 189, 201, 217, 233, and

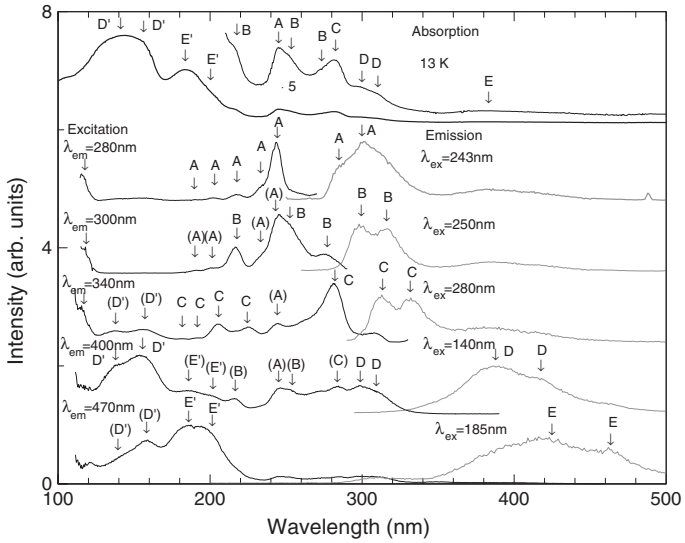

Figure 4. Fluorescence bands A–E observed in $SrMgF_4$:Ce excited at 243, 250, 280, 140 and 185 nm have double peaks. The excitation spectra of the A–C fluorescence bands consist of five resolved bands. The D and E fluorescence bands are red-shifted compared to the A–C fluorescence bands and their linewidths are fairly large. Arrows in the absorption, excitation, and fluorescence bands indicate peak positions.

243 nm. The strongest excitation band at 243 nm coincides with one of the absorption bands. The excitation spectrum obtained by monitoring the fluorescence intensity at $\lambda_{em} = 300$ nm includes both components of A and B excitation bands because of the overlap of the high energy component of the B fluorescence band and the low energy component of the A fluorescence band. New strong excitation bands, denoted by B, appear at 216, 251 and 274 nm, which are also in agreement with three bands (215, 250, 275 nm) in the absorption spectrum. The excitation spectrum for the low energy component ($\lambda_{em} = 340$ nm) of the C fluorescence band consists of five distinct bands with peaks at 181, 191, 206, 225, and 281 nm. In addition, the same weak excitation band with a peak at 120 nm for the A, B and C fluorescence bands is in agreement with that observed in isomorphous $BaMgF_4$:Ce:Na crystals, which is assigned to the band edge of the BMF crystal [8]. The excitation spectra obtained by monitoring the fluorescence intensities at $\lambda_{em} = 400$ and 470 nm are very similar to the absorption spectrum except for the relative intensities of the excitation bands below 200 nm. It is doubtful whether weak excitation bands observed in the range 210–290 nm can be assigned to D and E excitation bands, because their peaks are almost the same as those of the A, B, and C excitation bands. As a consequence, the excitation spectrum for the D fluorescence band ($\lambda_{em} = 400$ nm) is composed of new intense broadbands at 140 and 157 nm, denoted by D′, and new weak bands at 300 and 312 nm, denoted by D, being distinguished from the A, B and C excitation bands. In the same way, the excitation spectrum for the E fluorescence band ($\lambda_{em} = 470$ nm) is composed of 185 and 200 nm intense broadbands (E′), and a 380 nm weak broadband (E). These D′ and E′ excitation bands are in agreement with those in the absorption spectrum.

The fluorescence spectra in the SMF:Ce crystal with three excitation wavelengths of 280, 160, and 180 nm were observed in the range 17–300 K, as shown in figure 5. The relative intensities between the C and D fluorescence bands excited at 280 nm as shown in figure 5(a) are different from those shown in figure 4 because of the spectral response of the different monochromator and detector used. The fluorescence spectra observed at various

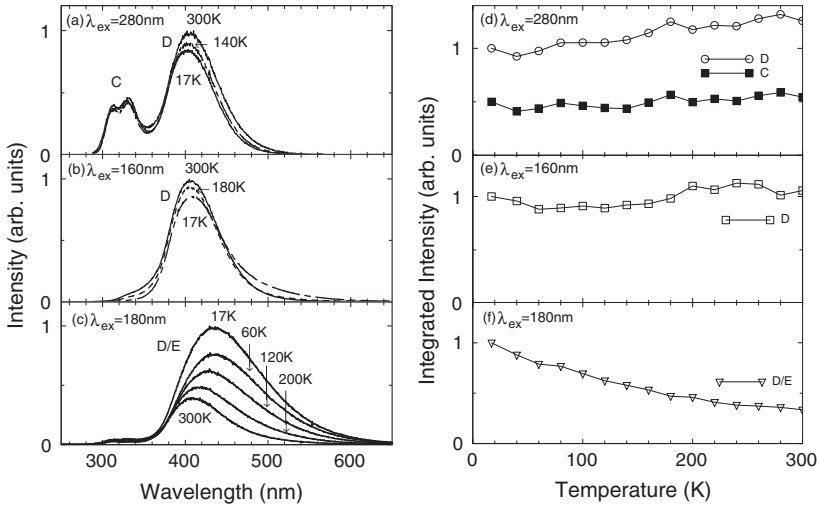

Figure 5. Temperature dependence of fluorescence spectra in $SrMgF_4$:Ce with 280, 160, and 180 nm excitation and their total intensities integrated in the wavelength domain.

temperatures shown in figures 5(a)–(c) are calibrated by dividing them by the excitation power. The linewidths of the D fluorescence spectra excited at 280 and 160 nm are slightly enhanced above 140 K. The integrated intensity over the spectral width of the fluorescence band for the (C, D) and D bands as shown in figures 5(d) and (e), respectively, are almost constant below 180 K and increase slightly by about 15% above 200 K with experimental uncertainty of about 10%. The slight increase of the intensities above 200 K may be due to the temperature dependence of the absorption coefficients and/or the refractive index. On the other hand, the D/E fluorescence bands excited at 180 nm, figure 5(c), gradually decrease in intensity and shift to shorter wavelengths with increasing temperatures from 17 to 300 K. The fluorescence intensity at 300 K is reduced to one-third compared to that at 17 K. The remaining band at 300 K is coincident with the D fluorescence band. These results suggest that the E fluorescence band with the peak at 430 nm decreases with an increase of temperature through a thermal non-radiative decay process [13] and disappears completely at 300 K.

The lifetime of the fluorescence as a function of wavelength measured at 300 and 13 K, which was excited at 266 and 290 nm from pulsed lasers and at 310 nm from a pulsed H_2 lamp, is presented in figure 6 together with the respective fluorescence spectrum. The relative intensities between the B and D fluorescence bands in figure 6(a) are also different from those in figure 4 for the same reason given above for figure 5. The lifetime of the B fluorescence band excited at 266 nm at 13 K is obtained to be 28 ns in the range 320–340 nm, whereas that of the D band increases gradually from 65 to 80 ns with wavelengths increasing from 350 to 440 nm, and is almost constant above 440 nm. Their lifetimes observed at 300 K are almost the same as those at 13 K. Figure 6(b) shows the lifetimes for the C and D fluorescence bands excited at 290 nm at 300 K and the integrated intensities of decay curves obtained by a streak camera as a function of wavelength. The lifetime for the C fluorescence band is almost constant (36 ns) in the range 310–340 nm, being slightly longer than that (28 ns) of the B fluorescence band. Figure 6(c) shows the lifetimes of only the D fluorescence band excited at 310 nm at 300 K. The lifetime of the D fluorescence band in figures 6(a)–(c) is almost the same. On the other hand, the lifetime of the E fluorescence band could not be measured because of there being no pulse laser source operating at 180–190 nm.

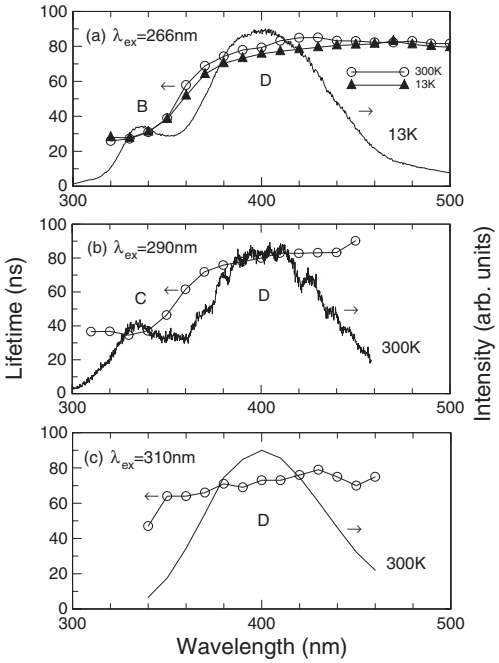

Figure 6. Lifetimes of the B, C and D fluorescence bands excited at 266, 290 and 310 nm and intensities integrated in the time domain as a function of fluorescence wavelength measured at 13 and 300 K in $SrMgF_4$:Ce.

The lifetimes of the B and D fluorescence bands measured at 300 K are the same as those at 13 K, indicating that their lifetimes are constant in this temperature range. This reveals that the non-radiative decay rates for these two centres are negligible for temperatures up to 300 K. The lifetime of the C fluorescence band was measured only at 300 K. However, the integrated intensities of the C and D fluorescence bands in figure 5 are almost constant over the temperature range 17–300 K, suggesting that the lifetime for this fluorescence band could also be relatively constant down to 17 K. As the optical properties of the A fluorescence band are very similar to those of the B and C fluorescence bands, the lifetime of the A fluorescence band is also anticipated to be constant below 300 K and of the similar order in magnitude as those of the B and C bands. The total absence of the E fluorescence band at 300 K suggests that phonon-assisted non-radiative decay for this centre is strong and dominates at temperatures above the base temperature of the present investigation at 17 K.

4. Discussion

4.1. Energy levels of Ce^{3+}

Optical absorption and excitation bands of Ce^{3+} ions correspond to electric dipole transitions from the $4f^1$ ground state to the $5d^1$ excited state. The ^2D excited states of Ce^{3+} polyhedra with C_{2v} in SMF are split into five nondegenerate Kramers doublets, giving rise to five resolved absorption/excitation bands. The energy levels of the $5d^1$ excited states are strongly modified by the crystal field consisting of cubic ($10Dq$) and low-symmetry components of Ce^{3+} polyhedra [13]. When the symmetry of the polyhedra changes from cubic to orthorhombic, the

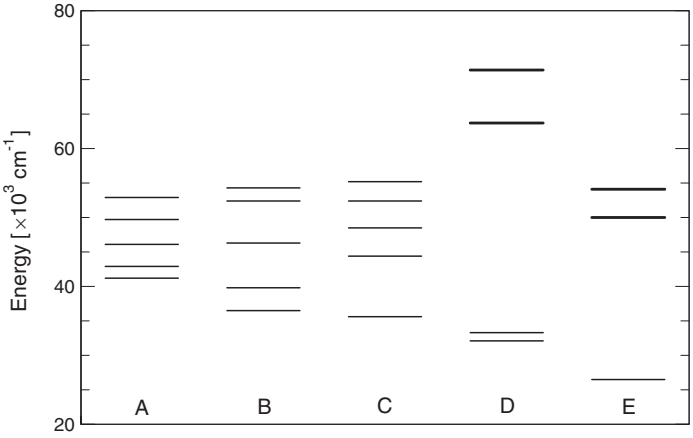

Figure 7. Schematic energy levels of excited states of A–E fluorescent centres. Energy levels represented by thin bars are calculated from the A–E excitation bands in figure 4. Thick bars represent energy levels corresponding to the D′ and E′ excitation bands.

five energy levels are spread, keeping the centre of gravity constant so that the lowest excited state shifts to lower energy [14].

The energy levels of the $5d^1$ excited states of Ce^{3+} polyhedra, estimated from the A, B and C excitation spectra composed of the five resolved bands at (189, 201, 217, 233, 243 nm), (184, 191, 216, 251, 274 nm) and (181, 191, 206, 225, 281 nm), respectively, are shown in figure 7. The energy levels of the lowest excited states shift to lower energy in alphabetical order. The centre of gravity between the five energy levels of the $5d^1$ excited states for the A, B and C centres, respectively, is obtained to be 46 600, 45 800, and 47 200 cm^{-1} and nearly equal to each other within experimental uncertainty. This reflects Ce^{3+} polyhedra with lowering of symmetry in descending order from A, B and C.

The excitation spectra for the D and E fluorescence bands in figure 4 are more complicated to analyse. The energy levels associated with the (D, D′) and (E, E′) excitation bands are shown in figure 7, in which the D′ and E′ levels are denoted by thick bars. The maximum energy separation (39 000 cm^{-1}) between the D′ and D bands is 2–3 times larger than those (12 000–20 000 cm^{-1}) observed for the A, B and C centres, which can be approximated to the crystal field splitting, $10Dq$, between the T_{2g} and E_g excited states of Ce^{3+} ions [13]. The intensity of the D′ (∼140 nm) band is much stronger than that of the D band (∼310 nm). This is opposite to the relative intensities of the excitation bands associated with the higher and lower excited states assigned to the A, B and C centres.

In order to examine the origin of the D/E fluorescence bands and the D′/E′ absorption bands, their optical properties are discussed in detail. First, we consider the lineshapes of the D and E fluorescence bands. The Ce^{3+} fluorescence spectrum from a single Ce^{3+} site should be decomposed into two Gaussians with the energy separation of 2200 cm^{-1}, being equal to the energy separation between the $^2F_{5/2}$ and the $^2F_{7/2}$ levels of the Ce^{3+} ions [13]. The dashed curves in figure 8 represent two Gaussians calculated through fitting the observed fluorescence bands in the energy scale. The energy separation of the A–C fluorescence bands with well-resolved double peaks is nearly equal (∼2000 cm^{-1}). The linewidths of the high and low energy components of the A–C bands are almost the same (∼680 and ∼970 cm^{-1}), respectively. On the other hand, the double peaks of the D and E fluorescence bands were not clearly resolved because of fairly large linewidth. Assuming that the D and E bands have the same separation of

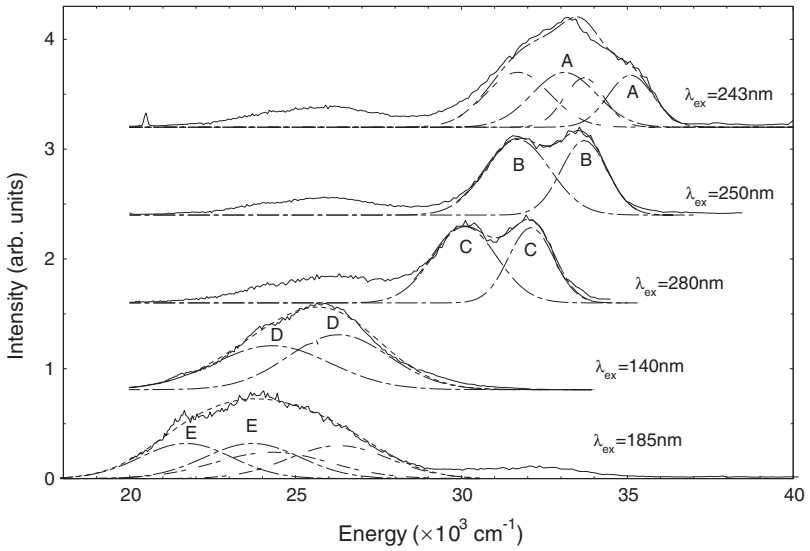

Figure 8. The lineshapes of the A–E fluorescence bands are decomposed into two Gaussians as a function of energy in the form $I(x) = \sum a_i \times \exp(-\frac{(x-x_i)^2}{2\sigma_i^2})$ with parameters a_i, x_i [$\times 10^3$ cm^{-1}] and σ_i [$\times 10^3$ cm^{-1}]. The fitting parameters (a_1, x_1, σ_1, a_2, x_2, σ_2) are obtained to be (0.78, 31.8, 1.3, 0.76, 34.0, 0.9), (0.76, 28.0, 1.2, 0.78, 30.3, 1.1) and (0.54, 22.2, 2.9, 0.52, 24.6, 2.4) for the A, B and C bands, respectively. The lineshapes of the D and E fluorescence bands are calculated with an assumption that the peak separation is about 2000 cm^{-1}, like those of the A–C bands. The fitting parameters are (0.4, 24.3, 1.74, 0.5, 26.3, 1.52) and (0.3, 21.7, 1.38, 0.3, 23.7, 1.44) for the D and E bands, respectively.

2000 cm^{-1}, the linewidths of the high and low components of the D and E bands are calculated to be (1520, 1740 cm^{-1}) and (1380, 1440 cm^{-1}), respectively. In summary, the D and E bands have fairly large red-shift compared to the A–C bands and fluorescence bandwidths, being roughly 1.5–2 times larger than those of the A–C bands. If the D and E bands are assumed to be due to Ce^{3+} ions similar to the A–C bands, then the D and E fluorescent centres with such large Stokes shift should have greater distortion than the A–C fluorescent centres.

Next, we consider the lifetimes of 28, 36, and 65–80 ns for the B, C and D fluorescence bands with the peaks at ∼320, ∼330 and ∼400 nm, respectively. Figure 9 shows the relation between the lifetimes and the peak wavelengths of Ce^{3+} fluorescence bands in various fluoride crystals including the SMF crystal. In a previous paper [15], we discussed the lifetimes of Ce^{3+} fluorescence in substitutionally disordered crystals of $CaNaYF_6$, where Ca^{2+}, Na^+, and Y^{3+} ions randomly occupy the common cation sites with the CaF_2-type cubic fluorite structure. The Ce^{3+} fluorescence band, with a fairly large width in the range 300–500 nm, shows inhomogeneous broadening, and the lifetimes are distributed in the range 35–90 ns. It has been concluded that the lifetimes are proportional to the fluorescence wavelengths, that is, a distribution of the lifetimes corresponds to a distribution of non-cubic components of the distortions created by the substitutional disorder [15]. The lifetimes of the B and C fluorescence bands satisfy the above relationship. On the other hand, the lifetime (75 ns) of the D fluorescence band (400 nm) lies on the extended straight line. So, it still satisfies the relationship. The D and E fluorescent centres are expected to be associated with Ce^{3+} polyhedra with large non-cubic components of the distortions.

Here, we propose a model for the D and E fluorescent centres associated with Ce^{3+} polyhedra. When trivalent Ce^{3+} ions substitute for divalent Sr^{2+} ions, charge compensators

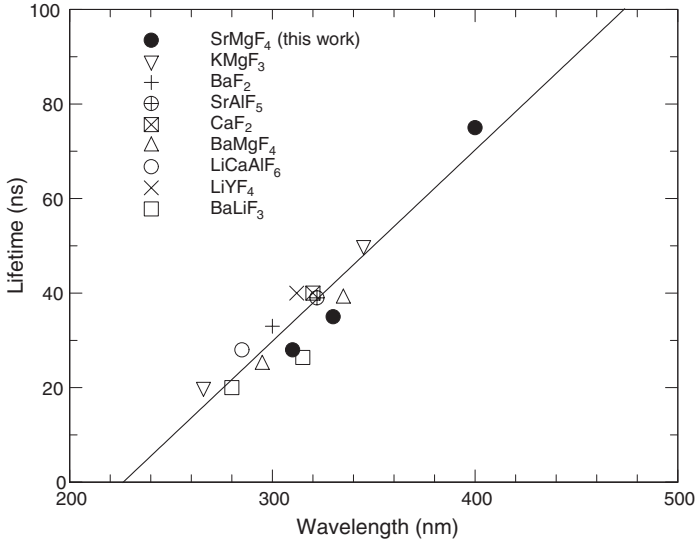

Figure 9. Lifetimes of Ce^{3+} fluorescence in various fluoride crystals [15]. The lifetimes of the B, C and D fluorescence bands in $SrMgF_4$:Ce are represented by solid circles. The straight line is only a guide to the eye.

are required because of keeping charge neutrality. Ce^{3+} polyhedra accompanied by charge compensators are expected to be largely distorted compared to the perfect Ce^{3+} polyhedra of the A–C centres. The SMF crystal used in this study includes only Ce^{3+} ions. Therefore, intrinsic charge compensators are proposed as follows.

(1) The first model is an interstitial F^- ion. The presence of interstitial F^- ions was found in rare-earth trivalent ion doped CaF_2 crystals using the ESR and ENDOR techniques [16]. The projection along the *a* axis in figure 2(b) suggests that there might be suitable cavities between Sr^{2+} ions. However, it is necessary to examine the existence of Ce^{3+} with an interstitial F^- ion by ESR measurements.

(2) The second model is cation vacancies, reported in Ce^{3+} doped $KMgF_3$ (KMF:Ce) [17, 18]. The absorption bands with double peaks at 227 and 236 nm and the single absorption band at 271 nm in KMF:Ce were assigned to optical transitions from the ground state to the lower $5d^1$ excited state of the perfect the Ce^{3+} ions with cubic symmetry and Ce^{3+} ions perturbed by K^+ vacancies located along the [001] axis, respectively. The existence of Ce^{3+} accompanied by a K^+ vacancy was confirmed by the ESR measurement [18]. The fluorescence from the perfect Ce^{3+} ions in KMF:Ce consists of bands with double peaks at 265 and 282 nm and with a lifetime of 22 ns, whereas that from the perturbed Ce^{3+} ions has a single broadband with a peak at 350 nm and with a lifetime of 50 ns [17]. A problem is whether this cation–vacancy model can explain the further red-shift of the D fluorescence band (400 nm) and the longer lifetime (75 ns). Another problem is whether the D′ and E′ intense absorption bands below 200 nm can be assigned to optical transitions to the higher $5d^1$ excited state of the Ce^{3+} ions. If the energy levels of the higher excited state approach the bottom of the conduction band, energy transfer from these levels occurs easily via the conduction band. Then, the intensities of the excitation bands corresponding to the higher excited state may be weaker than those corresponding to the lower excited state. This expectation is consistent with the relative intensities for the A–C excitation bands, but opposite to those of the D′ and D excitation bands.

(3) The third model is a fluorine vacancy with two electrons associated with a nearest Ce^{3+} ion. This model is the same as that proposed for photochromic (PC) centres observed in additively coloured CaF_2 doped with trivalent rare-earth ions (RE^{3+}) [9, 19–22]. The strength of the absorption bands corresponding to PC centres was reduced by UV irradiation (<400 nm), and new three bands shifting to higher energy appeared. This can be reversed either thermally or optically. Schematically, the photochemical reaction [19] may be described by $PC + RE^{3+} \overset{UV}{\underset{Vis,kT}{\Longleftrightarrow}} PC^{+} + RE^{2+}$. The PC^{+} centre ionized by UV irradiation was identified as an F_A centre (an electron trapped at a fluorine vacancy associated with a nearest neighbour RE^{3+} ion) by the ESR technique [20]. Recently, generation of the same absorption bands in CaF_2 containing Y^{3+} (∼5 ppm) by ArF excimer laser irradiation was reported [23]. As ESR signals from the F_A centre were observed simultaneously, the centre corresponding to the induced absorption bands seems to be the F_A centre. However, the concentration of the Y^{3+} impurity estimated from the ESR signal was much smaller than that calculated from the absorption bands. Therefore, it has been concluded that the major defects contributing to the optical absorption bands are two electrons trapped at a fluorine vacancy associated with Y^{3+}, whereas the minor defects sensitive to the ESR signals are an electron trapped a fluorine vacancy perturbed by Y^{3+} or Y^{2+}. In addition, a huge absorption band at ∼62 000 cm^{-1} (∼160 nm) was observed in the additively coloured CaF_2 crystals doped with RE^{3+} [22]. This band is interpreted as charge transfer from the PC centre to a nearby RE^{3+} ion. The intense broadbands with the double peaks at 140 and 157 nm in the SMF:Ce crystal are very similar to the broadbands with double peaks at 157 and 164 nm observed in the CaF_2:Ce crystal. If the D fluorescent centre is assumed to be a complex consisting of Ce^{3+} with two electrons trapped at a nearest neighbour fluorine vacancy, the Ce^{3+} complex is expected to be largely distorted, resulting in the large red-shift and the large linewidth of the D fluorescence band. However, as described above, there coexist PC and PC^{+} centres in the CaF_2 crystals. Therefore, the D fluorescence bands and the D′ absorption bands are interpreted as optical transitions from complexes consisting of Ce^{3+} and one or two electrons trapped at a vacancy of the nearest neighbour F^{-} ligand ions.

Finally, we discuss the origin of the E fluorescence band with the peak at 430 nm and the E′ absorption band with the peaks at 185 and 200 nm. If the E centre is associated with Ce^{3+} in a similar way as the D centre, the crystal field strength may be larger than that of the D centre. With increasing crystal field strength, the Stokes shift also increases, resulting in enhancement of phonon-assisted non-radiative decay rates below room temperature [13]. This expectation is consistent with the result in figure 5. The energy separation (∼6800 cm^{-1}) between the D (∼300 nm) and E (∼380 nm) absorption bands is very close to that (∼6000 cm^{-1}) between the A (∼240 nm) and C (∼280 nm) absorption bands. This fact suggests that the D and E centres consist of fluorine vacancies with one or two electrons associated with the A–C centres.

4.2. Superlattice structure and (A, B, C) centres

The x-ray diffraction from the SMF crystal indicates a superlattice structure with six distinct Sr^{2+} polyhedra, as shown in figure 3. Two groups of (Sr1, Sr2, Sr6) and (Sr3, Sr4, Sr5) are associated with strong and weak crystal fields, respectively, because the numbers of their ligand ions of the polyhedra are ten and nine.

The energy levels of the lowest $5d^1$ excited state of Ce^{3+}, estimated from the absorption/excitation bands for the A, B and C fluorescence bands are 41 100, 36 500 and 35 600 cm^{-1}, respectively. The maximum energy separation of the five excitation bands for the A, B and C centres is 12 000, 18 000 and 20 000 cm^{-1}, respectively, approximately equal to the crystal field splitting of 10 Dq. The stronger crystal field causes the larger splitting and

the larger red-shift. Then, the A and B/C fluorescent centres are associated with weak and strong crystal fields, respectively. As a consequence, the A absorption band is assigned to (Sr3, Sr4, Sr5), whereas the B and C absorption bands are assigned to (Sr1, Sr2, Sr6). Although the Sr2 polyhedron seems to be slightly different from the Sr1 and Sr6 polyhedra, it is difficult to explain the differences between the B and C absorption bands.

5. Conclusions

The x-ray diffraction for the SMF crystals indicates a superlattice structure. Five distinct fluorescence bands A–E were observed with different excitation wavelengths in the VUV and UV regions at low temperatures. Three fluorescence bands, A–C, have similar lineshapes and linewidths except for their peak shift. On the other hand, the other two bands D and E have larger red-shift and 1.5–2 times larger linewidths than those for the A–C bands. The A and (B, C) bands are assigned to the six Ce^{3+}-polyhedra with weak and strong crystal fields as a consequence of the superlattice structure in the SMF crystal, respectively. The D and E bands are interpreted as optical transitions from complexes consisting of Ce^{3+} ions and a one or two electron trapping vacancy of the nearest neighbour F^- ligand ions.

Acknowledgments

This work was in part supported by the Royal Society through the award of a joint research project between Japan and the UK.

References

[1] Moulton P F 1985 *Laser Handbook* vol 5, ed M Bass and M L Stitch (Amsterdam: North-Holland) p 282
[2] Blasse G and Grabmaier B C 1994 *Luminescent Materials* (Berlin: Springer)
[3] Ehrlich D J, Moulton P F and Osgood R M 1979 *Opt. Lett.* **4** 184
[4] Marshall C D, Speth J A, Payne S A, Krupke W F, Quarles G J, Castillo V and Chai B H T 1994 *J. Opt. Soc. Am.* B **11** 2054
[5] Misra P and Dubinskii M A (ed) 2002 *Ultraviolet Spectroscopy and UV Lasers* (New York: Dekker)
[6] Buchter S C, Fan T Y, Liberman V, Zayhowski J J, Rothschild M, Mason E J, Cassanho A, Jenssen H P and Burnett J H 2001 *Opt. Lett.* **26** 1693
[7] Yamaga M, Hattori K, Kodama N, Ishizawa N, Honda M, Shimamura K and Fukuda T 2001 *J. Phys.: Condens. Matter* **13** 10811
[8] Hayashi E, Ito K, Yabashi S, Yamaga M, Kodama N, Ono S and Sarukura N 2006 *J. Alloys Compounds* **408–412** 883
[9] Hayes W and Staebler D L 1974 *Crystals with the Fluorite Structure* ed W Hayes (Oxford: Clarendon) chapter 7
[10] Ishizawa N, Suda K, Etschmann B E, Oya T and Kodama N 2001 *Acta Crystallogr.* C **57** 784
[11] Banks E, Jenkins R and Post B 1982 *The Rare Earths in Modern Science and Technology* vol 3, ed G J McCarthy, H B Silber and J I Rhyne (New York: Plenum) p 329
[12] Kaminskii A A 1990 *Laser Crystals* (Berlin: Springer) (Table 2.1)
[13] Henderson B and Baryram R H 2000 *Crystal-Field Engineering of Solid-State Laser Materials* (Cambridge: Cambridge University Press)
[14] Kodama N, Yamaga M and Henderson B 1998 *J. Appl. Phys.* **84** 5820
[15] Yamaga M, Imai T, Miyairi H and Kodama N 2001 *J. Phys.: Condens. Matter* **13** 753
[16] Kiro D and Low W 1970 *Magnetic Resonance* ed C K Coogan, N S Ham, S N Stuart, J R Pilbrow and G V H Wilson (New York: Plenum) p 247
[17] Francini R, Grassano U M, Landi L, Scacco A, D'Elena M, Nikl M, Cechova N and Zema N 1997 *Phys. Rev.* B **56** 15109
[18] Yamaga M, Honda M, Kawamata N, Fujita T, Shimamura K and Fukuda T 2001 *J. Phys.: Condens. Matter* **13** 3461
[19] Staebler D L and Schnatterly S E 1971 *Phys. Rev.* B **3** 516
[20] Anderson C H and Sabisky E S 1971 *Phys. Rev.* B **3** 527
[21] Alig R C 1971 *Phys. Rev.* B **3** 536
[22] Loh E 1971 *Phys. Rev.* B **4** 2002
[23] Mizuguchi M, Hosono H, Kawazoe H and Ogawa T 1998 *J. Vac. Sci. Technol.* A **16** 3052